Chemical additive effect on asphaltenes destabilization and deposition studied using quartz crystal resonator (QCR) sensor: From atmospheric pressure titration to isothermal depressurization of non-diluted crude oil

Nelson Acevedo, Sadia Radji, Mohamed Saidoun, Frederic Tort, Jean-Luc Daridon

237 (2024) 212812

Contents lists available at ScienceDirect

Geoenergy Science and Engineering

journal homepage: www.sciencedirect.com/journal/geoenergy-science-and-engineering

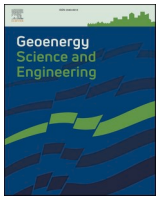

Chemical additive effect on asphaltenes destabilization and deposition studied using quartz crystal resonator (QCR) sensor: From atmospheric pressure titration to isothermal depressurization of non-diluted crude oil

Nelson Acevedo [a,1,*], Sadia Radji [b], Mohamed Saidoun [c], Frederic Tort [d], Jean-Luc Daridon [a,**]

[a] Université de Pau et des Pays de l'Adour, CNRS, TotalEnergies, LFCR, UMR 5150, E2S UPPA, Pau 64012, France
[b] Université de Pau et des Pays de l'Adour, CNRS, IPREM, Institut des Sciences Analytiques et de Physico- Chimie pour l'Environnement et les Matériaux, UMR 5254, E2S UPPA, Hélioparc, Pau 64053, France
[c] TOTAL S.E., CSTJF Research Center, 64018 Pau, France
[d] TotalEnergies Additives & Fuels Solutions, Givors 69700, France

ARTICLE INFO

Keywords:
Asphaltenes destabilization
High-pressure
Crude oil
QCR
Additive

ABSTRACT

In this study, the destabilization of asphaltenes in a crude oil sample was analyzed under various pressure conditions using a fully immersed Quartz Crystal Resonator (QCR) sensor. Firstly, oil samples with and without a chemical additive were tested at atmospheric pressure through titration with different liquid n-alkanes (C_7, C_9, and C_{12}) as antisolvents. Then, high-pressure experiments (HP) were conducted on a recombined crude oil + gas system, involving constant mass expansions from 1000 bar to the saturation pressure point at various fixed temperatures. From these high-pressure experiments, the phase diagrams, including the asphaltene pressure envelope (APE), were constructed and compared for the recombined oil with and without the chemical additive in both P vs T and P vs composition diagrams. The results regarding the impact of the chemical additive under HP conditions were compared with those obtained under atmospheric pressure conditions. The comparison shows an strong agreement between the two sets of experiments, confirming that the test conducted to evaluate the effectiveness of asphaltene inhibitors can be extrapolated to high-pressure applications.

1. Introduction

Asphaltenes can cause significant issues in the oil production process when they destabilize. This leads to self-association, phase transition and deposition on the surface of pipelines, wellbores, production systems, and transportation equipment. Their destabilization is triggered by changes in the surrounding conditions such a temperature, pressure, or composition variation (Gharbi et al., 2017). This deposition can result in decreased production rates, increased maintenance expenses, and even complete shutdowns of production facilities. These problems can be alleviated or prevented by utilizing additives that act as inhibitors for asphaltene destabilization. This, in turn, reduces costs and enhances the efficiency of oil production (Cenegy, 2001).

There are several types of additives employed in the oil industry to address the issues associated with asphaltene destabilization (Ansari et al., 2022). These additives include surfactants (Wiehe and Jermansen, 2003; Isaac et al., 2022; Alhreez and Wen, 2019), polymers (Subramanian et al., 2018a; Horeh et al., 2022), and co-solvents (Ali et al., 2022). Each type of additive operates in a distinct manner, ranging from impeding asphaltenes aggregation to preventing asphaltenes adsorption at surfaces. Regardless of their specific mechanism, their goal is always the same: to diminish or eliminate the propensity of asphaltenes to aggregate, precipitate, and deposit, thereby enhancing the stability of oil (Rogel, 2011).

Asphaltenes, as a complex polydisperse mixture of large, high molecular weight, and polar compounds, present a significant challenge in studying and understanding their destabilization process. The intricate nature of asphaltenes makes it difficult to determine their exact chemical structure, leading to complexities in characterizing their behavior and interactions within the crude oil (Chacón-Patiño et al., 2018;

* Corresponding author.
** Corresponding author.
E-mail address: nelson.acevedo@sorbonne-universite.fr (N. Acevedo).
[1] Current affiliation: Sorbonne Université, CNRS, Laboratoire Interfaces et Systèmes Electrochimiques, 4, place Jussieu, CP. 133, F-75005 Paris, France.

https://doi.org/10.1016/j.geoen.2024.212812
Received 21 August 2023; Received in revised form 22 March 2024; Accepted 30 March 2024
Available online 1 April 2024

Yarranton et al., 2013). Consequently, the interaction between asphaltenes and chemical additives, such as asphaltene deposition inhibitors, becomes a highly complex phenomenon as well, involving various factors such as π-π interactions, acid-base interactions, hydrogen bonding, complexing of metal ions and dipole–dipole interactions (Karambeigi et al., 2016; Smith et al., 2008; Madhi et al., 2017).

Given the ongoing demand for crude oil, the understanding of interactions between asphaltenes and additives assumes paramount importance in the development of new additives and improved formulations. The ultimate goal is to prevent asphaltene destabilization and deposition, enabling oil production processes with significantly reduced blockages and maintenance issues. However, the quest for simple and reliable laboratory-based techniques that can accurately assess the performance of additives under realistic oilfield conditions remains a desired yet complex task (Mojica et al., 2023; Juyal et al., 2022; Bae et al., 2016; Enayat et al., 2020).

Numerous studies have been conducted to assess chemical additives as inhibitors for asphaltene destabilization (Mojica et al., 2023; Campen et al., 2020; Yen et al., 2001; Khosravi et al., 2020; Ghloum et al., 2019). However, the majority of these studies were carried out under atmospheric condition using model solvents or diluted systems due to the challenges associated with evaluating additives in real crude oil under high-pressure reservoir conditions. Among the different techniques used to evaluate additives performance, sensor-based techniques using Quartz Crystal Resonators have recently gained prominence in investigating the impact of additives on inhibiting asphaltene adsorption and deposition (Subramanian et al., 2018a; Campen et al., 2019; Balestrin et al., 2019; El ghazouani et al., 2023; Cassiede et al., 2021a; Kahs et al., 2022; Raj et al., 2019). This probing technique can be easily implemented under high pressure conditions and have proven to be a reliable tool in the flow assurance field (Roshani et al., 2021).

The quartz crystal resonator technique was already employed to probe the destabilization of asphaltene in asphaltene dilute in toluene model solutions (Daridon et al., 2013) as well as to assess the ability of the model asphaltene compounds to form nanoaggregates in toluene and bigger flocs in heptols (Carrier et al., 2021). In the present study, the capabilities of quartz crystal probes were harnessed to examine the destabilization of asphaltenes in crude oil under both atmospheric and high-pressure conditions. The objective was to analyze the impact of a chemical additive during destabilization caused by depressurization in a recombined oil and to compare the results with those obtained in the atmospheric pressure titration of the dead oil. To achieve this objective, the first step involved investigating the destabilization of a crude oil sample under atmospheric pressure with and without the addition of an chemical additive. The destabilization and deposition of unstable materials were monitored during a titration process using a fully immersed Quartz Crystal Resonator sensor in oil samples. The titration was performed with three different liquid destabilizers (n-C7, n-C9, and n-C12). Next, experiments were conducted under high-pressure (HP) conditions on a recombined crude oil and gas mixture. A PVT cell with an integrated QCR sensor, fully immersed in the recombined oil sample, was used. A synthetic gas, representative of the gas found in the field, was used for the direct recombination of the crude oil in the measurement cell. Depressurization experiments were carried out from 1000 bar to the saturation pressure point by continuously expanding the fluid at constant mass and fixed temperature. From these HP experiments, the phase transitions corresponding to the saturation point pressure (L→L + V) and the upper asphaltene instability pressure (L→L + A) were determined. Phase diagrams, depicting fluid phase equilibria and the asphaltene pressure envelope (APE) of the recombined system with and without chemical additive, were then constructed in both pressure-temperature (P vs T) and pressure-composition (P vs composition) diagrams. Finally, the results concerning the effect of chemical additives obtained under HP conditions were compared with those obtained at atmospheric pressure conditions.

2. Materials and methods

2.1. Chemicals and materials

The dead crude oil and the synthetic gas used were provided by TotalEnergies, and its characteristic are summarized in Table 1 and Table 2, respectively. The chemical additive was provided by TotalEnergies Additives & Fuels Solutions. This additive is a polymer based on alkylphenol resins diluted in 50% of aromatic solvent. Once diluted, the polymer takes a liquid form. The functional groups present are phenolic groups with branched hydrocarbon side chains. The alkylphenol resin is modified with an alkyl polyamine introducing some secondary amine functions on the polymer. The concentration of polymer is set at 50 % m/m. Pure toluene (>99.8), n-heptane (C7) (>99%) and n-nonane (C9) (>99%) were acquired from Fisher Scientific, n-dodecane (C12) (>99%) was acquired from Sigma Aldrich. The n-alkanes were used as destabilizing agent for atmospheric-pressure titration experiments, whereas the synthetic gas was used for recombination with dead oil to carry out depressurization experiments.

2.2. Sample preparation

2.2.1. Addition of chemical additive in crude oil sample

Whether conducting experiments at atmospheric pressure or high pressure, the oil samples used in the study required a volume of approximately 20 cm^3. This posed challenges in accurately adding the chemical additive in parts per million (ppm) by weight. To address this challenge, a double dissolution method was implemented. Initially, the chemical additive was dissolved in a toluene solution to create an additive stock solution with the desired concentration for achieving the intended final proportion in the oil. Subsequently, a portion of this solution, corresponding to a mass fraction of approximately 2%, was injected into the oil samples. To avoid introducing any bias caused by the addition of toluene to the oil, the same quantity of toluene was also injected into the oil used for experiments without the additive. This allowed for a proper comparison of results. After preparation, the oil sample mixed with chemical additives is subjected to agitation at 70 °C for 24 h prior to commencing the experiments.

2.2.2. Addition of chemical additive in n-alkane antisolvents

In order to avoid the dilution effect on the content of chemical additive during the titration process, a consistent mass fraction of the additive was maintained in the liquid mixture that was in contact with the sensor. To accomplish this, the chemical additive was also added to the titrant tank. This involved dissolving the necessary quantity of additive directly into the respective n-alkane (heptane, nonane, or dodecane) and subjecting it to ultrasound for 5 min prior to utilization.

2.2.3. Oil and gas recombination

Prior to each high-pressure experiment, the pressure within the PVT cell was reduced using a vacuum pump, and the cell wall was cooled down to 4 °C. Simultaneously, the crude oil sample (or the crude oil with

Table 1
Selected properties of the Crude Oil sample.

Properties of the Crude Oil	
Wax Appearance Temperature (°C)	33
$Density_{65°C}$ ($Kg.m^{-3}$)	953.8
$Viscosity_{65°C}$ ($mPa.s^{-1}$)	136.5
$Asphaltenes_{C7}$ (wt %)	17.5
ASI 100 (Passade-Boupat et al., 2013) (C7 wt %)	40–45
Molecular Weight ($g.mol^{-1}$)	268
Reservoir Temperature (°C)	108
Well-head Temperature (°C)	67
GOR[a] (Sm (Ansari et al., 2022)/Sm^{-3})	80–90

[a] GOR of the reservoir fluid.

Table 2
Composition of the Synthetic Gas, determined by Gas Chromatography.

Composition of the Synthetic Gas	
Compound	Mol %
N_2	4.002
CO_2	9.381
Methane	53.654
Ethane	15.698
Propane	11.569
Iso-Butane	1.480
n-Butane	4.216

the addition of the chemical additive) was heated at a temperature of 70 °C to prevent wax precipitation. Following this, the crude oil was introduced into the cell gravimetrically using suction, and the mass of the injected crude oil was determined using an analytical balance. Afterwards, the required amount of gas was injected into the cell at a temperature of 30 °C using a syringe pump. The mass of the injected gas was calculated by converting the volume change of the syringe pump into mass, with the density data for the gas obtained from the NIST REFPROP software. Finally, the prepared mixture was heated to the operating temperature and rapidly brought to the higher pressure of the constant mass expansion experiment. At this pressure, the system was thoroughly mixed under stirring while continuously monitoring the resonant parameters of the quartz senor. This was done to observe the equilibration of both the recombined system and the sensor, and most importantly, to ensure that the asphaltenes did not destabilize prior to the initiation of the depressurization process.

2.3. Instrumental setup and technique

Similar to our previous studies (Cassiede et al., 2021a; Carrier et al., 2021), two different experimental setups utilizing the QCR sensor were employed to investigate the destabilization of the sample. These setups include an atmospheric-pressure device and a high-pressure PVT cell. Both experimental setups employed the same type of sensor, which is a thickness shear resonator comprising an AT-cut beveled quartz disk. The sensor has a nominal resonance frequency of 3 MHz and a blank diameter of 13.6 mm. On the central plano-plano portion of the disk, two electrodes were deposited through vacuum evaporation. The deposition process involved applying a 10 nm thick layer of titanium as an adhesive, followed by a 100 nm thick layer of gold. The objective of both apparatus is to record the oscillation parameters of the quartz sensor immersed in the studied system in order to calculate the shift in resonance frequency (Δf_n) and the change in half-band-half-width ($\Delta \Gamma_n$) with respect to initial conditions, which are indicative of the alterations in the surrounding medium during asphaltenes destabilization. Using a network analyzer, the resonance frequencies f_n were measured for various overtone ($n = 1,3,5$ and 7) with an uncertainty of 4 Hz, while the resonance half-band half-width Γ_n (related to resonator damping) was determined with a standard uncertainty of 5 Hz.

The shift in resonance can be primarily attributed to contributions from mass loading $\Delta f_{n,m}$ given by Sauerbrey (1959) law and liquid (viscous) loading $\Delta f_{n,\eta}$ as described by Kanazawa's relation (Keiji Kanazawa and Gordon, 1985) according to the following combination:

$$\Delta f_n = \underbrace{-n\,2C_m\Delta m}_{\text{mass loading}} \underbrace{-\sqrt{n}\,C_m(\pi f_0)^{-1/2}\sqrt{\rho\eta}}_{\text{Liquid Loading}} \quad \text{(Eq 1)}$$

where C_m is the Sauerbrey's constant, Δm is the estimated deposited mass on the quartz active surface, $\rho\eta$ is the density-viscosity product of the quartz surface surrounding media, f_0 is the fundamental frequency of the QCR in air at $T = 25$ °C (2999302 Hz for the sensor used here). On the other hand, $\Delta \Gamma_n$, which is associated with energy dissipation, is predominantly influenced by liquid loading according to the following relation:

$$\Delta \Gamma_n = \underbrace{\sqrt{n}\,C_m(\pi f_0)^{-1/2}\sqrt{\rho\eta}}_{\text{Liquid Loading}}(1+R) \quad \text{(Eq 2)}$$

Here, R is an empirical correction term that accounts for viscous friction on real roughness electrode surfaces. Further details regarding the theoretical description of Quartz Crystal Microbalance parameters and the model utilized in this study can be found in our previous publications (Daridon et al., 2013, 2020; Acevedo et al., 2020).

Since the QCR technique relies on the indirect identification of discontinuities during phase transitions, experiments need to be conducted by monitoring the changes in the resonant behavior of the quartz sensor, specifically Δf_n and $\Delta \Gamma_n$, induced by variations in any of the thermodynamic variables. In studies conducted under atmospheric pressure, the composition of the dead oil is altered by continuously adding an antisolvent during titration. In studies conducted under atmospheric pressure, the composition of the dead oil is modified by continuously adding an antisolvent during titration. Meanwhile, in experiments involving a recombined oil + gas system, the variable changed is the pressure by performing constant mass expansions starting from the higher pressure of the study. The decrease in pressure or the quantity of antisolvent needed to reach the detection threshold, commonly known as the onset of flocculation, is influenced by both the aging time of the system and the sensitivity of the equipment used for detection. The lower the sensitivity of the sensor, the later the onset is detected. Hence, it becomes crucial to utilize sensors that operate on the scale relevant to the phenomena under investigation. In the case of asphaltene, which operates on the nanometer scale, the QCR sensor is well suited given its operational range in that scale. To address kinetic effects, when using techniques sensitive in the micrometer like optical or centrifugation methods, Maqbool et al., 2009, 2011 have introduced approaches that account for solution aging such as microscopic time detection and time-resolved centrifugation. While these techniques haven't been directly applied to QCR sensors, in our investigation of inhibitor efficiency involving a comparison with and without inhibitors, we have maintained consistent oil disruption kinetics. This involves a depressurization rate of 0.3 MPa/min and antisolvent addition at 0.25 g/min.

The crude oil sample under investigation reveals the presence of waxes, which possess the potential to precipitate. Such precipitation can introduce complications in the indirect detection of asphaltene destabilization conducted by monitoring QCR sensors. In order to mitigate these potential issues, measurements were carried out at higher temperatures that the wax appearance temperature. In any case, in scenarios where asphaltene destabilization and wax precipitation could occur under study conditions, an effective strategy for differentiating these phenomena is to plot the ratio $-\Delta f_n/\Delta \Gamma_n$. As the quartz sensor is fully immersed in oil, there is no thermal gradient between the sensor surface and the surrounding oil and consequently wax deposition does not occur. As a result, $-\Delta f_n/\Delta \Gamma_n \approx 1$. Conversely, in the case of asphaltene destabilization, deposition occurs, leading to $-\frac{\Delta f_n}{\Delta \Gamma_n} > 1$. Therefore, the ratio value proved (Daridon et al., 2020) effective in differentiating asphaltene destabilization and wax precipitation.

2.3.1. Atmospheric-pressure device and titration experiments

The atmospheric-pressure experimental device has been fully detailed in previous works (El ghazouani et al., 2023; Daridon et al., 2013; Acevedo et al., 2020; Cassiede et al., 2021b; Acevedo et al., 2021; Saidoun et al., 2019). It mainly consists of a thermoregulated titration cell which contains the quartz sensor fully immersed in the sample fluid studied and a magnetic bar for an efficient mixing of the system during titrant addition. A peristaltic pump is utilized to ensure a constant flow rate of 0.25 g/min for adding the titrant (either n-alkane or n-alkane + Additive Destabilizing solution). However, the amount of antisolvent added is measured by weighing the antisolvent tank.

Before the titration experiment begins, the temperature of the experimental cell was set to 70 °C and this temperature was kept con-

stant during the whole titration. The frequency (f_n) and half-band-half-width (Γ_n) for the harmonics $n = 3$, 5, 7, and 9 of the QCR sensor in air are recorded. These measurements provide reference values for the resonance properties of the unloaded quartz. Then, the titration begins by adding 22.0 g of either Crude Oil or Crude Oil + chemical additives to the titration cell. Once the resonance frequency of the sensor reaches a stable value within a range of ±1 Hz, the titrant is added by turning on the peristatic pump. Throughout the entire experiment, the response of the QCR sensor to changes in oil properties is continuously monitored and recorded using a Network analyzer.

To facilitate the comparative analysis with and without the addition of a chemical additive in crude oil, the experiments were conducted using the same QCR sensor. Therefore, special attention was given to the cleaning of the quartz surface. With this objective in mind, after each titration experiment, the sensor was washed in pure toluene and placed in an ultrasonic bath at 50 °C for 10 min to remove any asphaltene deposits. Subsequently, it was dried using an inert gas. During the washing process and the storage of the sensor between successive experiments, any direct contact with the quartz surface was avoided. Furthermore, before each new titration experiment, the resonance properties of the quartz in air were recorded and compared to the initial values. This step was taken to ensure proper cleaning and to verify the absence of any damage to the quartz surface caused by bending or scratching, which could potentially affect the reference values.

2.3.2. High-Pressure device and depressurization experiments

The high-pressure device has been also presented in details in some previous works (Carrier et al., 2021; Daridon et al., 2020; Cassiede et al., 2021b; Saidoun et al., 2019; Cardoso et al., 2014). It consists of a PVT cell with a movable piston that allows for varying pressure from 0.1 to 1000 bar. This volumetric cell is equipped with a precise position sensor that enables the recording of volume variations with a relative uncertainty of 0.05%. Inside the cell, a quartz crystal disk is integrated using HP electrical feedthroughs. This sensor is fully immersed in the sample fluid under study, which is homogenized by two magnetic stirring bars placed inside the cell. To measure the pressure of the fluid, a pressure gauge is employed in direct contact with the fluid within the cell, ensuring that no part of the fluid is isolated from the sensing area. The pressure gauge is calibrated against a primary standard pressure sensor, providing an accuracy of better than 0.02% within the pressure range of 0.1–100 MPa. Furthermore, to maintain a constant temperature, a heat-carrier liquid is circulated through channels arranged in the vessel wall. This heat-carrier liquid is connected to a thermostat bath circulator. Temperature measurements are carried out using a platinum resistance implanted in the body of the PVT cell, with an uncertainty of better than 0.1 K. Additionally, a vacuum pump and a syringe pump are connected to the setup to allow for the recombination of the oil and gas as detailed in the previous section.

After preparing the oil and gas mixture and allowing it to reach equilibrium, the depressurization experiment commences by gradually expanding the volume of the cell at a constant depressurization rate of 3 bar/min. Throughout the depressurization process, the sensor's signal is continuously monitored to calculate the shifts in resonance frequency and half-band-half-width for the fundamental and three overtones (3rd, 5th, 7th). Simultaneously, the pressure, volume, and temperature of the fluid inside the cell are measured and recorded. These data are used to plot the changes in resonance frequency, dissipation, and volume as a function of pressure. These plots help identify any anomalies or trends indicative of phase transitions.

The resonant frequencies and half-band-half-width values in air are also recorded at each temperature prior to every experiment. These measurements serve to calculate the shift in resonant properties resulting from full immersion in the high-pressure fluid. Subsequently, the hydrostatic effects on resonance frequency (Cassiède et al., 2010) ($\Delta f_{n,P}$) are subtracted from Δfn to isolate the influence of fluid contact on the quartz surface, allowing for an accurate observation of changes in both resonant frequency and damping. Moreover, following this correction, the change in resonance frequency (Δf_{ncorr}) caused by fluid load becomes comparable to studies conducted at atmospheric pressure, enabling the use of the same equations (Eqs. (1) and (2)). Similarly, to the atmospheric studies, the high-pressure experiments are repeated under the same operational conditions, both with and without the presence of chemical additives. By directly comparing the resulting curves with and without the additive, the performance of the additive at different concentrations can be evaluated.

3. Results and discussion

3.1. Atmospheric-pressure dead crude oil destabilization

To assess the impact of the chemical additive on the destabilization of asphaltenes, titration experiments were first carried out at atmospheric pressure at 70 °C using a fully immersed QCR. Different n-alkanes were employed as titrants on the dead crude oil sample, both with and without the additive. Initially, the concentration of the additive was evaluated using n-heptane as the titrant. Subsequently, the effect of the additive in the presence of different destabilizing agents was examined using n-nonane and n-dodecane, and the results were compared with those obtained using n-heptane.

3.1.1. Additive concentration effect

The destabilization of the crude oil sample was achieved using n-heptane as the destabilizing agent, and it was monitored using the sensor response. Fig. 1 shows the frequency shifts of the 3rd harmonic (Δf_3) and the deposited mass (Δm) during the titration of the dead crude oil, both with (dotted curves) and without the chemical additive (solid curve). In this figure, the frequency shifts were directly obtained by subtracting the frequency measured at initial conditions (pure oil sample after stable signal) and the frequency measured at each composition value during titration. On the other hand, Δm was calculated from the slope of the plot of $\Delta f_n/\sqrt{n}$ versus $\sqrt{n}$ the square root of the harmonic number according to Eq. (1).

It can be seen in Fig. 1a that the frequency shift initially increases as a result of the viscosity and density reduction caused by adding n-heptane to the system. As Subsequently, a progressive reduction of the signal is observed as the sample destabilization begins, followed by a sudden decrease in the signal, indicating the deposition of unstable asphaltenes on quartz surface. This trend is further supported by the Δm plot in Fig. 1b, where it can be observed that shortly after reaching the composition of 60 mol% of C7, there is a significant increase in the amount of deposited material, corresponding to the precipitated asphaltenes.

When comparing the response of the sensor with different additive concentrations in Fig. 1a and b, it becomes evident that at a low concentration (200 ppm), the sensor cannot detect any significant difference in the onset of destabilization (60 mol% C7) or in the deposited mass compared to the sample without the additive (represented by the black continuous curve). However, when the additive concentration is increased to 2000 ppm, an improvement in the stability of the mixture is observed. This improvement is reflected in the increased amount of titrant required for destabilization, which rises from 60 to 63 mol%. It is important to note, though, that there is no reduction in the amount of deposited material at the end of the titration, which corresponds to 85 mass% of titrant added.

In a previous publication (El ghazouani et al., 2023), similar results were obtained in a titration of a crude oil with n-heptane using an additive at various concentrations. At a low concentration of additive (300 ppm), a negative (almost zero) deposition inhibition efficiency (−5.91%) was observed, whereas at higher concentrations of additive, such as 3000 ppm, the inhibition efficiency increased to 61%. However, in the system studied here, the additive does not inhibit the deposition of asphaltenes but instead increases the system's stability by delaying the

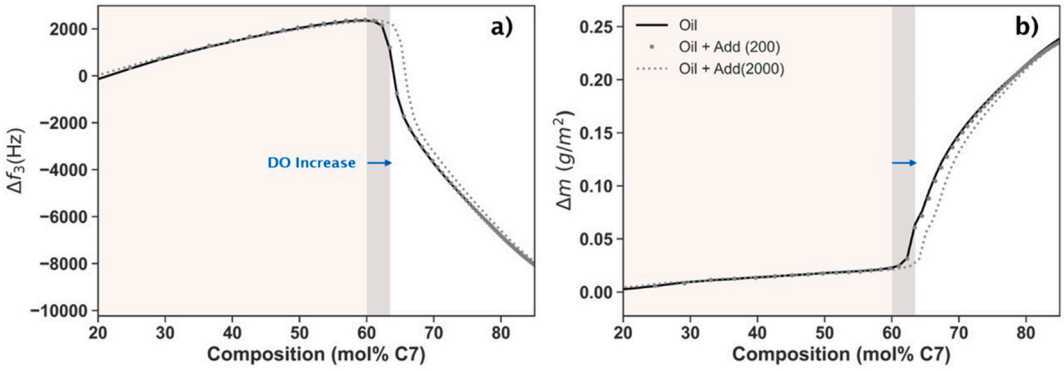

Fig. 1. QCR titration curves for the *Crude Oil* (−) and *Oil + Additive Mixtures* (Oil + Add) at different concentrations: (●) 200 ppm and (…) 2000 ppm. a) Frequency shifts (Δf_3) of the third harmonic and b) Deposited Mass (Δm) on the quartz surface vs composition of n-heptane.

onset of destabilization.

3.1.2. Additive effect on different destabilizing agents

Based on the previous results, the effect of the additive was evaluated on different destabilizing agents using a working concentration of 2000 ppm. Fig. 2 presents a comparison of the frequency shifts of the 3rd harmonic (Δf_3) and the deposited mass (Δm) during the titration of the dead crude oil with different n-alkanes: n-heptane (represented by black-gray curves), n-nonane (represented by yellow curves), and n-dodecane (represented by blue curves), with and without the additive (represented by dotted and plain curves, respectively).

When comparing the effect of the n-alkane used for destabilization (in chain length range: C7–C12), it can be observed that as the carbon chain size increases, the destabilization onset (DO, expressed in mol% of n-alkane) decreases as well. Although destabilization begins earlier for dodecane than heptane, fewer asphaltenes are destabilized (Fig. 2b) and consequently, deposition appears less severe with increasing the carbon number in the n-alkane chain, being the deposition tendency C12 < C9 < C7. These results are consistent with those reported previously (Calles et al., 2008; Hu and Guo, 2001), where the amount of precipitated asphaltenes using different n-alkanes decreased with an increase in the carbon number.

Furthermore, the results in Fig. 2 indicate that the effect of the additive on the destabilization onset remains consistent, resulting in an increase of 3 mol% of titrant for the Destabilization Onset (DO) regardless of the n-alkane used. Moreover, there is no significant reduction in the amount of deposited material observed at the end of the titration.

3.2. Depressurization of the recombined live crude oil

For the depressurization experiments, three temperatures (65 °C, 85 °C, and 108 °C) were studied based on the operating temperatures shown in Table 1. Five compositions were examined for the system Crude Oil + Gas and Oil/Additive + Gas: 20, 41, 54, 65, and 68 mol% of gas. Similarly to the previous section, concentrations of 200 and 2000 ppm were used for the additive in the Oil + Additive samples. The determinations of the liquid-vapor saturation pressure (Psat) corresponding to either L/L + V or L + A/L + A + V transitions, as well as the upper asphaltenes instability pressure (UAIP) corresponding to asphaltene separation from the liquid phase L/L + A, were performed by analyzing the Δf_{3corr} and ΔΓn vs. P curves during the depressurization, as reported in previous works (Daridon et al., 2020; Saidoun et al., 2019), in this analysis, Δfncorr represents the value of Δf_n corrected by subtracting the change in frequency due to pressure effect ($\Delta f_3, P$). As an example, Fig. 3 illustrates the depressurization of the Crude Oil + Gas system (65 mol %). The deviation from the linear trend in the signal of (Δf_{ncorr} is considered as the UAIP, as it has been demonstrated to indicate the appearance of unstable asphaltenes in previous studies works (Saidoun et al., 2019; Daridon and Carrier, 2017). It can be seen in this figure that the sensor demonstrates a substantial response (2500 Hz) to asphaltene separation, which is most pronounced at the saturation point. At this point, a sharp change occurs, highlighted by an angular point, revealing the appearance of bubbles in oil + destabilized asphaltenes systems.

The values of upper asphaltenes instability pressure and liquid-vapor saturation pressure obtained for the system at the three temperatures were plotted in the P,x phase diagrams shown in Fig. 4 it can be seen that by increasing the amount of gas in the system the UAIP rises whatever the temperature investigated. This indicates that the risk of asphaltenes

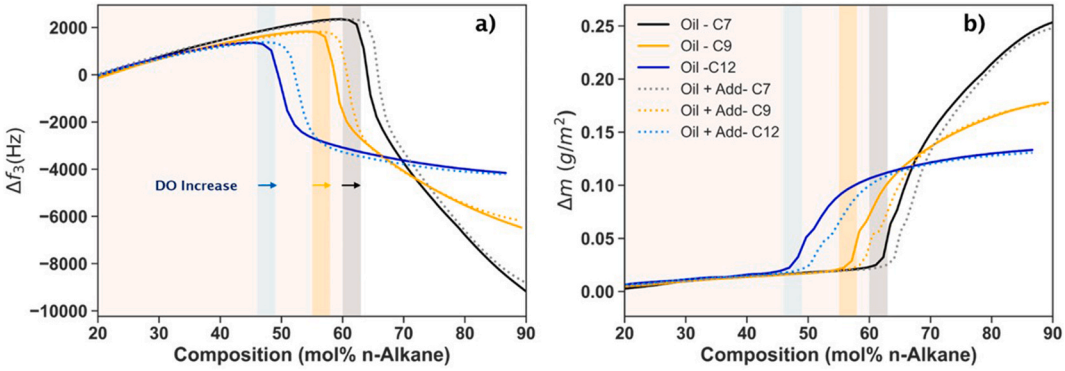

Fig. 2. QCR titration curves for the Crude Oil (−) and Oil + Additive Mixture 2000 ppm with different n-alkanes as destabilizing agent: n-heptane (Black curves), n-nonane (yellow curves) and n-dodecane (blue curves). a) Frequency shifts (Δf_3) of the third harmonic and b) Deposited Mass (Δm) on the quartz surface vs composition of n-alkane.

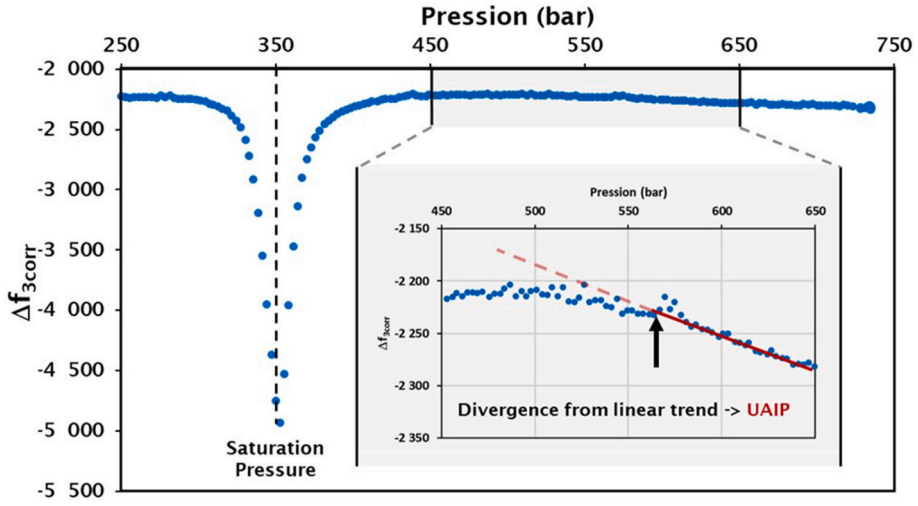

Fig. 3. Saturation Pressure (Psat) and UAIP determination from the Δf_{3corr} values during depressurization of the system Crude Oil + Gas (65 mol%) at 108 °C.

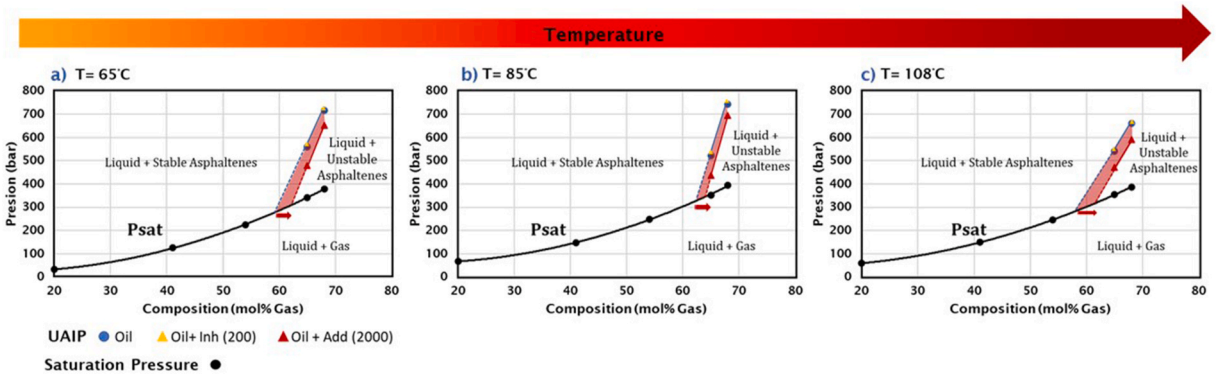

Fig. 4. Pressure vs composition phase diagrams for recombined Oil + Gas (blue ●), Oil + Additive (200 ppm) + Gas (yellow ▲) and Oil + Additive (2000 ppm) + Gas (red ▲) at 65 (a), 85 (b) and 108 °C (c).

destabilization increases with higher gas content in the system. By extrapolating the linear trend of the UAIP (—) until it intersects with the Psat curve (represented by black ●), the minimum gas content required to destabilize asphaltenes in solution was estimated. For the system without Additive, the estimated values range between 59 and 62 mol% of gas. The use of Additive at low concentration (200 ppm) has no effect on the values of UAIP, confirming the results obtained at atmosferic pressure. However, at a concentration of 2000 ppm, there is a decrease observed in the UAIP at all temperatures studied. As a result, the intersection with the Psat curve is altered, requiring an increased amount of gas (2–4 mol%) to destabilize asphaltenes. This indicates that the Additive interacts favorably with the asphaltenes in solution, keeping them in a stable state even at higher gas compositions. Of course, due to the small quantities incorporated, the addition of additives at these levels has no effect on the liquid-vapor saturation curve.

The effect of the addition of the chemical additive in recombined oil even more noticeable when looking at the pressure rather than the shift in injected gas content. For this reason, the reduction in UAIP due to the

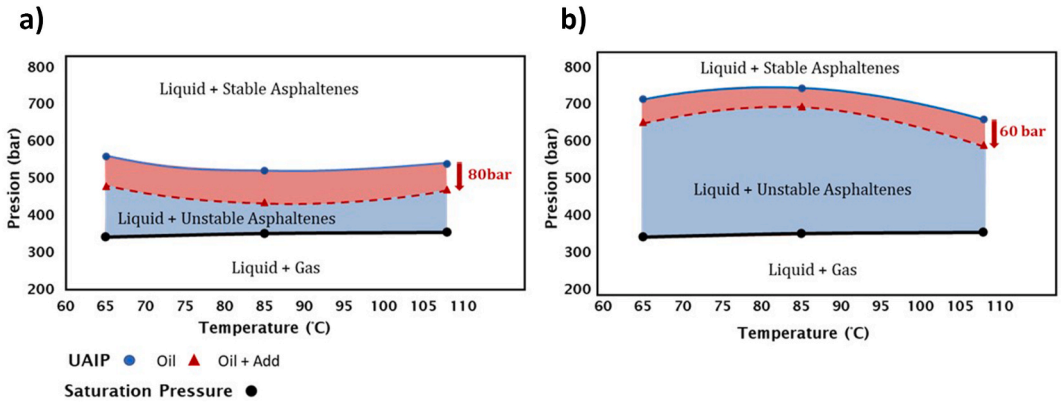

Fig. 5. Pressure vs Temperature diagrams for recombined Oil + Gas (blue ●) and Oil + Additive + Gas (red ▲). a) 65 and b) 68%mol gas.

addition of the Additive at a concentration of 2000 ppm, for the temperatures studied, is presented in Fig. 5a and Fig. 5 b, which represent Pressure vs Temperature diagrams for 65 mol% gas and 68 mol% gas, respectively.

In the case of 65 mol% gas, the asphaltenes instability domain is reduced by approximately 42%, occurring around 80 bar. However, for 68 mol% gas, the reduction occurs at around ~60 bar, resulting in only a 19% decrease. This indicates that the effectiveness of the Additive is dependent on the composition of the system. At higher gas concentrations, the impact of the additive is less pronounced.

As in the case of atmospheric pressure titrations, the estimation of the deposited mass (Δm) on the sensor during the depressurization experiment was made possible through the analysis of multiple harmonics. The plots of obtaned Δm vs P can be found in the supporting information.

Table 3 presents a comparison of the maximum value of Δm (Δm Max) for the system with and without Additive during the depressurization for compositions of 65 mol% and 68 mol% gas at different temperatures. It is evident from these figures that the Additive not only reduces the asphaltenes instability domain but also significantly decreases the amount of asphaltenes deposited on the sensor. The reduction is more pronounced at low gas composition (65 mol% gas) compared to 68 mol% gas, where the reduction ranges from 23% to 52%.

These results are fully consistent with those obtained at atmospheric pressure (see Fig. 2), where the additive has a greater impact on reducing the amount of deposited asphaltenes on the sensor at concentrations closer to the destabilization onset (DO). However, for higher concentrations of the destabilizing agent, this reduction is not significant.

3.3. Comparison of high pressure with atmospheric pressure experiments

The results obtained from both sets of experiments, atmospheric pressure titration of the dead crude oil and isothermal depressurization of the recombined oil using the QCR technique to evaluate the effect of an additive on asphaltenes destabilization, show good correlation between them. These experiments provide consistent qualitative and quantitative insights into the influence of the chemical additive on asphaltene destabilization. Firstly, the results indicate that the addition of the additive at a low concentration (200 ppm) does not influence enough asphaltenes destabilization or deposition to be detectable by the quartz sensor. However, at a higher concentration (2000 ppm), there is a notable increase in the stability of asphaltenes in the crude oil, resulting in a delay in the onset of destabilization during titration or constant mass expansion experiments. This effect is observed regardless of the destabilizing agent used, whether it is C7, C9, or C12 for atmospheric pressure titration, or a Synthetic Gas mixture (C1+C2+C3+C4 = 87%, CO2+N2 = 13%) for depressurization experiments.

Secondly, it was seen in both cases that the addition of the chemical additive leads to a significant reduction in the amount of asphaltenes deposited on the QCR sensor in proximity to the destabilization threshold conditions. However, whether at atmospheric or high pressure, as the concentration of the antisolvent increases, the decrease in deposition becomes less pronounced, eventually becoming negligible for a highly destabilized system (>75 mol% n-alkane). These observations can be interpreted in two ways.

i. The concentration of the additive may be insufficient compared to the total amount of asphaltenes far from the onset, resulting in the additive being unable to interact with the newly formed aggregates once the unstable asphaltenes exceed its capability. It is important to note, however, that while this situation could potentially occur during depressurization experiments, which are conducted at a constant mass, it is less likely to happen during titration in atmospheric pressure experiments. In the latter case, efforts were made to maintain a constant additive concentration in order to avoid dilution bias. This was achieved by continuously increasing the amount of additive in the system with the addition of the destabilizing agent. Consequently, in this case there is always a renewal of free chemical additive that can interact with the asphaltenes likely to destabilize far from the threshold.
ii. ii. The additive selectively interacts with a small fraction of asphaltenes, specifically targeting the most unstable ones. This interaction prevents their destabilization and deposition, consequently delaying the onset of destabilization to higher concentrations of the titrant. However, when the concentration of the destabilizing agent reaches a certain threshold, the more stable asphaltenes destabilize independently, without any affinity for the additive. Consequently, these asphaltenes aggregate and deposit on the QCR sensor, resulting in no discernible difference in mass between the destabilization of an additive-free oil and an oil + additive mixture.

The latter scenario is not surprising considering the high polydispersity of asphaltenes. This polydispersity leads to varying degrees of interaction between chemical additives and different fractions of the asphaltenes. In their publication, Subramanian et al. demonstrated that only a small fraction (approximately 6%) of the studied asphaltenes strongly interacts with a commercial fatty-alkylamine inhibitor. This proportion of interacting species was found to be higher in the subfraction of irreversibly-adsorbed asphaltenes, which mainly consists of acidic asphaltenes (Subramanian et al., 2018b). Fig. 6 illustrates the interaction strength of the additive with the asphaltenic fraction of the crude oil studied here.

Table 3
– Comparison of the Maximum Deposited Mass (Δm Max) during depressurization experiments between the pure oil and the oil + Additive mixture at 65 and 68 mol % Gas.

Composition (mol% Gas)	Temperature (°C)	Δm Max ($g.m^{-2}$)		Reduction (%)
		Oil	Oil + Additive	
65	65	0.68	0.24	66.20
	85	0.47	0.09	80.85
	108	0.26	0.02	92.31
68	65	0.81	–	–
	85	0.66	0.51	22.73
	108	0.54	0.26	51.85

4. Conclusions

A comparison was conducted to evaluate the effect of an additive on asphaltenes destabilization using two different experimental setups: atmospheric pressure titration of dead crude oil and depressurization of recombined live crude oil using a fully immersed Quartz Crystal Microbalance (QCR). The obtained results showed a strong correlation between the two sets of experiments for the additive and the system under study. At a low additive concentration (200 ppm), no significant effect on asphaltenes destabilization or deposition was observed. However, at a higher concentration (2000 ppm), the additive acted as a retardant, delaying the destabilization process and increasing the amount of antisolvent required destabilizing agent required for initiate destabilization by approximately 3 mol%, regardless of the n-alkane used (C7, C9, or C12) for atmospheric pressure titration or Synthetic Gas for depressurization experiments. Regarding the deposition of unstable asphaltenes, the use of the additive led to a substantial reduction in deposited material during the early stages of destabilization. However, this effect became less pronounced as the content of the destabilizing agent increased. This indicates that the additive primarily interacts with the most unstable asphaltenes, which constitute only a small fraction of the total asphaltene content in the oil.

These findings suggest that atmospheric pressure titrations with n-

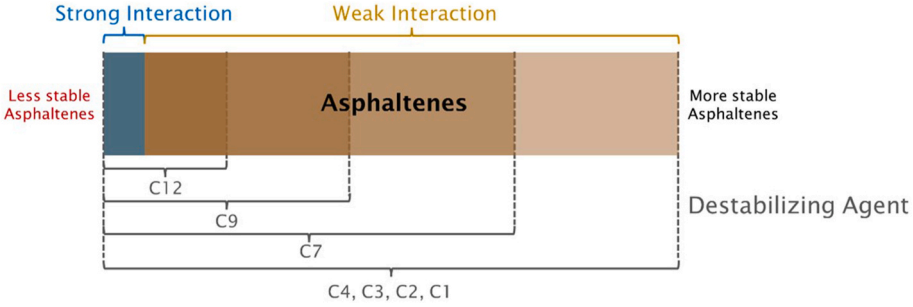

Fig. 6. Additive interaction with asphaltenes.

alkanes can be extrapolated to isothermal depressurization experiments with live crude oil, which provide more representative conditions for oilfield applications. Nevertheless, there remains uncertainty in predicting field inhibitor performance based on laboratory testing alone. Therefore, future studies using different additives and crude oil samples are necessary to confirm the effectiveness of this approach.

Notes

The authors declare no competing financial interests.

CRediT authorship contribution statement

Nelson Acevedo: Writing – review & editing, Writing – original draft, Methodology, Investigation, Formal analysis. **Sadia Radji:** Validation, Investigation. **Mohamed Saidoun:** Validation, Resources, Investigation. **Frederic Tort:** Validation, Resources, Investigation. **Jean-Luc Daridon:** Formal analysis, Conceptualization, Funding acquisition, Investigation, Project administration, Validation, Writing – original draft, Writing – review & editing.

Declaration of competing interest

The authors declare that they have no known competing financial interests or personal relationships that could have appeared to influence the work reported in this paper.

Data availability

The authors do not have permission to share data.

Appendix A. Supplementary data

Supplementary data to this article can be found online at https://doi.org/10.1016/j.geoen.2024.212812.

References

Acevedo, N., Moulian, R., Chacón-Patiño, M.L., Mejia, A., Radji, S., Daridon, J.L., Barrère-Mangote, C., Giusti, P., Rodgers, R.P., Piscitelli, V., Castillo, J., Carrier, H., Bouyssiere, B., 2020. Understanding asphaltene fraction behavior through combined quartz crystal resonator sensor, FT-ICR MS, GPC ICP HR-MS, and AFM characterization. Part I: extrography fractionations. Energy Fuel. 34 (11), 13903–13915. https://doi.org/10.1021/acs.energyfuels.0c02687.

Acevedo, N., Vargas, V., Piscitelli, V., Bouyssiere, B., Carrier, H., Castillo, J., 2021. SiO 2 biogenic nanoparticles and asphaltenes: interactions and their consequences investigated by QCR and GPC-ICP-HR-MS. https://doi.org/10.1021/acs.energyfuels.0c04185.

Alhreez, M., Wen, D., 2019. Molecular structure characterization of asphaltene in the presence of inhibitors with nanoemulsions. RSC Adv. 9 (34), 19560–19570. https://doi.org/10.1039/c9ra02664a.

Ali, S.I., Awan, Z., Lalji, S.M., 2022. Laboratory evaluation experimental techniques of asphaltene precipitation and deposition controlling chemical additives. Fuel 310 (PA), 122194. https://doi.org/10.1016/j.fuel.2021.122194.

Ansari, F., Shinde, S.B., Paso, K.G., Sjöblom, J., Kumar, L., 2022. Chemical additives as flow improvers for waxy crude oil and model oil: a critical review analyzing structure-efficacy relationships. Energy Fuel. 36 (7), 3372–3393. https://doi.org/10.1021/acs.energyfuels.1c03747.

Bae, J., Fouchard, D., Garner, S., Macias, J., 2016. Advantages of applying a multifaceted approach to asphaltene inhibitor selection. Proc. Annu. Offshore Technol. Conf. 4, 3298–3307. https://doi.org/10.4043/27171-ms.

Balestrin, L.B.D.S., Francisco, R.D., Bertran, C.A., Cardoso, M.B., Loh, W., 2019. Direct assessment of inhibitor and solvent effects on the deposition mechanism of asphaltenes in a Brazilian crude oil. Energy Fuel. 33 (6), 4748–4757. https://doi.org/10.1021/acs.energyfuels.9b00043.

Calles, J.A., Dufour, J., Marugán, J., Peña, J.L., Giménez-Aguirre, R., Merino-García, D., 2008. Properties of asphaltenes precipitated with different N-alkanes. A study to assess the most representative species for modeling. Energy Fuel. 22 (2), 763–769. https://doi.org/10.1021/ef700404p.

Campen, S., Moorhouse, S.J., Wong, J.S.S., 2019. Mechanism of an asphaltene inhibitor in different depositing environments: influence of colloid stability. J. Pet. Sci. Eng. (September), 106502 https://doi.org/10.1016/j.petrol.2019.106502.

Campen, S., Moorhouse, S.J., Wong, J.S.S., 2020. Mechanism of an asphaltene inhibitor in different depositing environments: influence of colloid stability. J. Pet. Sci. Eng. 184. https://doi.org/10.1016/j.petrol.2019.106502. September 2019.

Cardoso, F.M.R., Carrier, H., Daridon, J.L., Pauly, J., Rosa, P.T.V., 2014. CO2 and temperature effects on the asphaltene phase envelope as determined by a quartz crystal resonator. Energy Fuel. 28 (11), 6780–6787. https://doi.org/10.1021/ef501488d.

Carrier, H., Daridon, J., Simon, S., Sj, J., Cassie, M., 2021. Comparing C5Pe and asphaltenes under temperature and pressure reservoir conditions using an acoustic wave sensor. https://doi.org/10.1021/acs.energyfuels.0c04397.

Cassiède, M., Daridon, J.-L., Paillol, J.H., Pauly, J., 2010. Impedance analysis for characterizing the influence of hydrostatic pressure on piezoelectric quartz crystal sensors. J. Appl. Phys. 108 (3), 1–8. https://doi.org/10.1063/1.3460805.

Cassiede, M., Mejia, A., Radji, S., Carrier, H., Daridon, J.L., Saidoun, M., Tort, F., 2021a. Evaluation of the influence of a chemical inhibitor on asphaltene destabilization and deposition mechanisms under atmospheric and oil production conditions using QCM and AFM techniques. Energy Fuel. 35 (21), 17551–17565. https://doi.org/10.1021/acs.energyfuels.1c02570.

Cassiede, M., Mejia, A., Radji, S., Carrier, H., Daridon, J., Saidoun, M., Tort, F., 2021b. Evaluation of the influence of a chemical inhibitor on asphaltene destabilization and deposition mechanisms under atmospheric and oil production conditions using QCM and AFM techniques. https://doi.org/10.1021/acs.energyfuels.1c02570.

Cenegy, L.M., 2001. Survey of Successful World-wide Asphaltene Inhibitor Treatments in Oil Production Fields. Proc. - SPE Annu. Tech. Conf. Exhib., pp. 1831–1837. https://doi.org/10.2523/71542-ms

Chacón-Patiño, M.L., Rowland, S.M., Rodgers, R.P., 2018. The compositional and structural continuum of petroleum from light distillates to asphaltenes: the boduszynski continuum theory as revealedby FT-ICR mass spectrometry. ACS Symp. Ser. 1282, 113–171. https://doi.org/10.1021/bk-2018-1282.ch006.

Daridon, J.-L., Carrier, H., 2017. Measurement of phase changes in live crude oil using an acoustic wave sensor: asphaltene instability envelope. Energy Fuel. 31 (9), 9255–9267. https://doi.org/10.1021/acs.energyfuels.7b01655.

Daridon, J.-L., Cassiède, M., Nasri, D., Pauly, J., Carrier, H., 2013. Probing asphaltene flocculation by a quartz crystal resonator. Energy Fuel. 27 (8), 4639–4647. https://doi.org/10.1021/ef400910v.

Daridon, J.L., Lin, C.W., Carrier, H., Pauly, J., Fleming, F.P., 2020. Combined investigations of fluid phase equilibria and fluid-solid phase equilibria in complex CO2-crude oil systems under high pressure. J. Chem. Eng. Data 65 (7), 3357–3372. https://doi.org/10.1021/acs.jced.0c00144.

El ghazouani, J., Saidoun, M., Tort, F., Daridon, J.L., 2023. Experimental evaluation method of asphaltene deposition inhibitors' efficacy at atmospheric pressure using a fully immersed quartz crystal resonator, centrifugation, and optical microscopy techniques. Energy Fuel. https://doi.org/10.1021/acs.energyfuels.3c00305.

Enayat, S., Tavakkoli, M., Yen, A., Misra, S., Vargas, F.M., 2020. Review of the current laboratory methods to select asphaltene inhibitors. Energy Fuel. https://doi.org/10.1021/acs.energyfuels.0c02554.

Gharbi, K., Benyounes, K., Khodja, M., 2017. Removal and prevention of asphaltene deposition during oil production: a literature review. J. Pet. Sci. Eng. 158 (August), 351–360. https://doi.org/10.1016/j.petrol.2017.08.062.

Ghloum, E.F., Rashed, A.M., Safa, M.A., Sablit, R.C., Al-Jouhar, S.M., 2019. Mitigation of asphaltenes precipitation phenomenon via chemical inhibitors. J. Pet. Sci. Eng. 175 (December 2018), 495–507. https://doi.org/10.1016/j.petrol.2018.12.071.

Horeh, N.B., Hosseinpour, N., Bahramian, A., 2022. Asphaltene inhibitor performance as a function of the asphaltene molecular/aggregate characteristics: evaluation by interfacial rheology measurement and bulk methods. Fuel 2023 339, 127420. https://doi.org/10.1016/j.fuel.2023.127420 (November.

Hu, Y.F., Guo, T.M., 2001. Effect of temperature and molecular weight of N-alkane precipitants on asphaltene precipitation. Fluid Phase Equilib. 192 (1–2), 13–25. https://doi.org/10.1016/S0378-3812(01)00619-7.

Isaac, O.T., Pu, H., Oni, B.A., Samson, F.A., 2022. Surfactants employed in conventional and unconventional Reservoirs for enhanced oil recovery—a review. Energy Rep. 8, 2806–2830. https://doi.org/10.1016/j.egyr.2022.01.187.

Juyal, P., Enayat, S., Lucente-Schultz, R., Li, Q., Karimipour, M., Tavakkoli, M., Cao, T.B., Yen, A., Russell, C., Vargas, F.M., 2022. Case study: investigation of the performance of an asphaltene inhibitor in the laboratory and the field. Energy Fuel. 36 (4), 1825–1831. https://doi.org/10.1021/acs.energyfuels.1c03557.

Kahs, T., Raj, G., Whelan, J., Larkin, E., Commins, P., Punnapala, S., Odeh, N., Abdallah, D., Naumov, P., 2022. Evaluation of the effectiveness of inhibitors for middle eastern asphaltenes by quartz crystal microbalance with dissipation. Energy Fuel. 36 (16), 8786–8798. https://doi.org/10.1021/acs.energyfuels.2c00365.

Karambeigi, M.A., Nikazar, M., Kharrat, R., 2016. Experimental evaluation of asphaltene inhibitors selection for standard and reservoir conditions. J. Pet. Sci. Eng. 137, 74–86. https://doi.org/10.1016/j.petrol.2015.11.013.

Keiji Kanazawa, K., Gordon, J.G., 1985. The oscillation frequency of a quartz resonator in contact with liquid. Anal. Chim. Acta 175 (C), 99–105. https://doi.org/10.1016/S0003-2670(00)82721-X.

Khosravi, R., Rodriguez, C., Mostowfi, F., Sieben, V., 2020. Evaluation of crude oil asphaltene deposition inhibitors by surface plasmon resonance. Fuel 273 (March). https://doi.org/10.1016/j.fuel.2020.117787.

Madhi, M., Bemani, A., Daryasafar, A., Khosravi Nikou, M.R., 2017. Experimental and modeling studies of the effects of different nanoparticles on asphaltene adsorption. Pet. Sci. Technol. 35 (3), 242–248. https://doi.org/10.1080/10916466.2016.1255641.

Maqbool, T., Balgoa, A.T., Fogler, H.S., 2009. Revisiting asphaltene precipitation from crude oils: a case of neglected kinetic effects. Energy Fuel. 23 (7), 3681–3686. https://doi.org/10.1021/ef9002236.

Maqbool, T., Raha, S., Hoepfner, M.P., Fogler, H.S., 2011. Modeling the aggregation of asphaltene nanoaggregates in crude oil-precipitant systems. Energy Fuel. 25 (4), 1585–1596. https://doi.org/10.1021/ef1014132.

Mojica, D., Angeles, M., Alvarez, O., Pradilla, D., 2023. Asphaltene precipitation and the influence of dispersants and inhibitors on morphology probed by AFM. Colloids and Interfaces 7 (1), 3. https://doi.org/10.3390/colloids7010003.

Passade-Boupat, N., Zhou, H., Rondon-Gonzalez, M., 2013. Asphaltene Precipitation From Crude Oils : How To Predict It And To Anticipate Treatment? Soc. Pet. Eng., 164184 https://doi.org/10.2118/164184-ms.

Raj, G., Larkin, E., Lesimple, A., Commins, P., Whelan, J., Naumov, P., 2019. In situ monitoring of the inhibition of asphaltene adsorption by a surfactant on carbon steel surface. Energy Fuel. 33 (3), 2030–2036. https://doi.org/10.1021/acs.energyfuels.8b04246.

Rogel, E., 2011. Effect of inhibitors on asphaltene aggregation: a theoretical framework. Energy Fuel. 25 (2), 472–481. https://doi.org/10.1021/ef100912b.

Roshani, M.M., Rostaminikoo, E., Joonaki, E., Mirzaalian Dastjerdi, A., Najafi, B., Taghikhani, V., Hassanpouryouzband, A., 2021. Applications of the quartz crystal microbalance in energy and environmental sciences: from flow assurance to nanotechnology. August Fuel 2022 313, 122998. https://doi.org/10.1016/j.fuel.2021.122998.

Saidoun, M., Palermo, T., Passade-Boupat, N., Gingras, J.P., Carrier, H., Daridon, J.-L., 2019. Revisiting asphaltenes instability predictions by probing destabiliztion using a fully immersed quartz crystal resonator. Fuel 251 (February), 523–533. https://doi.org/10.1016/j.fuel.2019.04.025.

Sauerbrey, G., 1959. Use of vibrating quartz crystals for thin film weighing and microweighing. Zeitschrift für Phys. 155 (2), 206–222. https://doi.org/10.1007/BF01337937.

Smith, D.F., Klein, G.C., Yen, A.T., Squicciarini, M.P., Rodgers, R.P., Marshall, A.G., 2008. Crude oil polar chemical composition derived from FT-ICR mass spectrometry accounts for asphaltene inhibitor specificity. Energy Fuel. 22 (5), 3112–3117. https://doi.org/10.1021/ef800036a.

Subramanian, S., Buscetti, L., Simon, S., Sacré, M., Sjöblom, J., 2018a. Influence of fatty-alkylamine amphiphile on the asphaltene adsorption/deposition at the solid/liquid interface under precipitating conditions. Energy Fuel. 32 (4), 4772–4782. https://doi.org/10.1021/acs.energyfuels.8b00059.

Subramanian, S., Simon, S., Sjöblom, J., 2018b. Interaction between asphaltenes and fatty-alkylamine inhibitor in bulk solution. J. Dispers. Sci. Technol. 39 (2), 163–173. https://doi.org/10.1080/01932691.2017.1304221.

Wiehe, I.A., Jermansen, T.G., 2003. Design of synthetic dispersants for asphaltenes. Pet. Sci. Technol. 21 (3–4), 527–536. https://doi.org/10.1081/LFT-120018536.

Yarranton, H.W., Ortiz, D.P., Barrera, D.M., Baydak, E.N., Barre, L., Frot, D., Eyssautier, J., Zeng, H., Xu, Z., Dechaine, G., Becerra, M., Shaw, J.M., Mckenna, A. M., Mapolelo, M.M., Bohne, C., Yang, Z., Oake, J., 2013. On the size distribution of self-associated asphaltenes. https://doi.org/10.1021/ef400729w.

Yen, Andrew, Yin, Y. Ralph, and Samuel Asomaning. "Evaluating Asphaltene Inhibitors: Laboratory Tests and Field Studies." Paper presented at the SPE International Symposium on Oilfield Chemistry, Houston, Texas, February 2001. doi: https://doi.org/10.2118/65376-MS.